RESEARCH ARTICLE

ADVANCED
ELECTRONIC
MATERIALS
www.advelectronicmat.de

Check for updates

Interfacial Control via Reversible Ionic Motion in Battery-Like Magnetic Tunnel Junctions

Guofei Long, Qian Xue, Qiang Li,* Yu Shi, Lin Li, Long Cheng, Peng Li, Junwei Zhang, Xixiang Zhang, Haizhong Guo, Jing Fu, Shandong Li,* Jagadeesh S. Moodera, and Guo-Xing Miao*

Electrical control on interfaces is one of the key approaches to harvest advanced functionalities in modern electronic devices. In this work, it is proposed and demonstrated that a "battery-like" tunnel junction structure can be embedded with added control and functionalities via reversible lithium-ion motion. In a model system of FeCo/FeCoO$_x$/LiF/FeCo magnetic tunnel junctions, the ultrathin LiF barrier makes strong electric fields possible under moderate applied voltages, and can therefore electrically drive reversible lithium-ion migration within the barrier. The ion motion subsequently leads to reversible interfacial modifications that generates over a thousand percent resistance change across the devices. Meanwhile, sizable tunneling magnetoresistance persists and even reverses the sign of spin polarization as a function of the interfacial control. The devices are therefore responsive to both electric and magnetic field manipulations, giving rise to diverse and nonvolatile functionalities.

1. Introduction

Modern electronic devices are progressively getting more and more sophisticated, and thus, additional control and functionalities are always in high demand for better integrity and portability. Interface engineering is one of the most important approaches to realize such goals because "the interface is the device."[1] With most devices' performance depends sensitively on the interfacial chemistry and structure; as such the electrical control over interfacial behavior promises new functionalities and device concepts.[2–5] Being the smallest cation ion with high ionic mobility, lithium ions have already played a key role in energy storage applications.[6] Here we utilize the Li ion battery concept in a drastically different context, for a new type of lithium ionic device.[7] With the tunable and nonvolatile motion of lithium ions through an ultrathin dielectric barrier, we show that multiple resistance states can be written to the cell with added control and functionalities, demonstrating potential applications for information storage and logic device terminal controls.

It is well known that lithium containing materials can exchange ions with transition metal oxides, leading to notable changes in their magnetic and electric properties.[8–9] Our conceptual heterojunction, as shown in **Figure 1**, consists of an ultrathin lithium-containing dielectric layer plus a transition metal oxide layer forming a composite barrier. The lithium dielectric layer can provide mobile lithium ions, analogous to the solid-state electrolyte in lithium ion batteries, but requiring strong enough applied electric fields for the ion motion activation. The interfacial oxide layer serves as the ion reservoir

G. Long, Q. Xue, Q. Li, Y. Shi, L. Li, L. Cheng, P. Li, G.-X. Miao
Institute for Quantum Computing & Department of Electrical
and Computer Engineering
University of Waterloo
Ontario N2L 3G1, Canada
E-mail: liqiang@qdu.edu.cn; guo-xing.miao@uwaterloo.ca
Q. Xue, Q. Li, S. Li, G.-X. Miao
College of Physics Science
Qingdao University
Qingdao 266071, China
E-mail: liqiang@qdu.edu.cn; lishd@qdu.edu.cn;
guo-xing.miao@uwaterloo.ca
J. Zhang, X. Zhang
Division of Physical Science and Engineering
King Abdullah University of Science & Technology (KAUST)
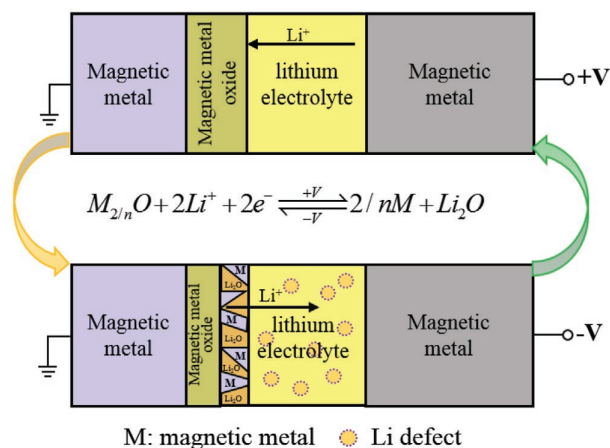Thuwal 23955-6900, Saudi Arabia

H. Guo
Department of Physics and Microelectronics
Zhengzhou University
Zhengzhou 450001, China
J. Fu
School of Materials Science and Engineering
Key Laboratory of Advanced Civil Engineering Materials of Ministry of
Education
Tongji University
Shanghai 201804, China
J. S. Moodera, G.-X. Miao
Department of Physics
Plasma Science and Fusion Center and Francis Bitter Magnet Laboratory
Massachusetts Institute of Technology
Cambridge, MA 02139, USA

**ADVANCED
SCIENCE NEWS**
www.advancedsciencenews.com

**ADVANCED
ELECTRONIC
MATERIALS**
www.advelectronicmat.de

Figure 1. Design concept of a battery-like magnetic tunnel junction under electric field-driven migration of lithium ions. An ultrathin, lithium-containing dielectric barrier serves simultaneously as quantum tunnel barrier as well as the solid-state "electrolyte" in such structures.

(analogous to an anode) to capture and release the ions through surface redox reactions, as shown in the formula in Figure 1. The reversible ionic exchange in the composite barrier under electric fields has two clear functionalities. Firstly, ionic exchange can lead to non-volatile resistance changes, analogous to the memristor behavior from the resistive switching (RS) effect.[10–19] At the same time, the thin tunnel barrier also permits direct quantum mechanical tunneling, and stable resistance states from the tunnel magnetoresistance (TMR) effect[20–26] also manifest themselves. Secondly, ionic migration leads to electrical control on the interfacial magnetic properties,[27,28] which further influences the spin-polarized transport and even reverses its polarity as the interfacial modification progresses. The parent compound we used, LiF, does not produce RS on its own because dielectric breakdown kicks in before that. But introducing a thin "cathode" (oxides in our system) layer to accept ions resolved this issue. Comparing to approaches such as combing TMR with ferroelectricity to obtain multistates,[29–31] our "battery-like" concept borrowed from electrochemistry can keep the layers ultrathin and makes a promising route to create large TMR and large RS but low impedance and low operation voltages for practical devices. Our scheme of driving lithium ion motion for interfacial control adds considerable versatility into existing tunnel junction devices, and opens up vast possibilities for designing improved devices with more advanced functionalities.
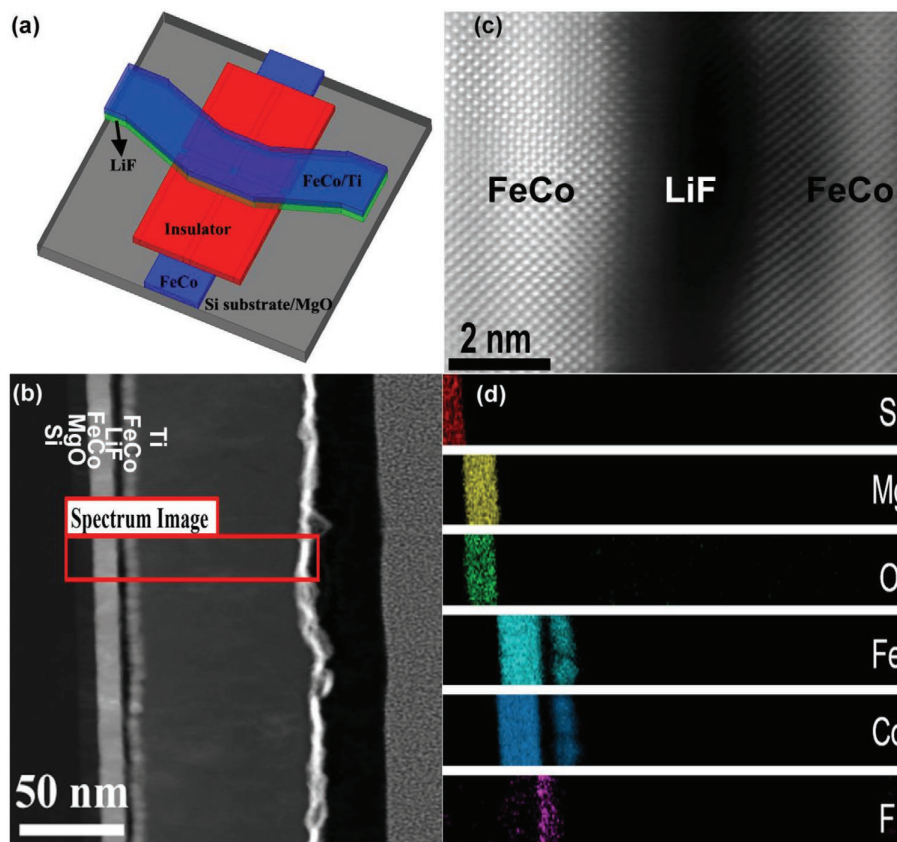
2. Results and Discussion

A schematic layout of the device is illustrated in **Figure 2**a. The top and bottom magnetic layers were chosen to have very different thicknesses (8 and 3 nm, respectively) in order to separate their switching fields. $Fe_{50}Co_{50}$ was selected because of its high intrinsic spin polarization.[24] We start by looking at the cross-sectional overview of the pristine device (Figure 2b), which reveals well-defined layers throughout. Specifically, the LiF is well formed and continuous. Symmetric and off-axis

X-ray diffraction clearly showed that the top FeCo layer is overall oriented with occasional misalignments, indicating that LiF is also mostly oriented (Figure S1 in the Supporting Information, but directly imaging the lattice structures of the LiF layer was difficult because of the extremely light elements). Experimentally, too thin LiF leads to shorted junctions, while too thick would fully suppress quantum tunneling: we found a nominal thickness of 2.8 nm (calibrated by quartz crystal microbalance) to be the optimum thickness and thus used it throughout this work. From Figure 2c, we can clearly see well-crystalized (100) lattice structures of FeCo electrodes with occasional misalignments. Figure 2d shows the electron energy loss spectroscopy (EELS) mapping of Si, Mg, O, Fe, Co, and F over the marked area of Figure 2b, consistent with the structure of the MTJs.

Figure 3a–c shows the TMR loops of tunnel junctions with progressively increasing interfacial natural oxidation time (3, 6, and 12 h, respectively). The oxidation also sets the as-deposited devices in the relatively high resistance states (HRS). As the oxidation time increases, the tunnel junction resistance increases and the TMR decreases. These evidenced that oxidation indeed took place in our system. Here, the TMR ratio is defined as TMR (%) = $(R_{AP} - R_p)/R_p \times 100\%$, where R_{AP} (R_p) is the junction resistance when the magnetization directions of the two ferromagnetic layers are antiparallel (parallel) to each other. As a comparison, the TMR behavior of a near-pristine device with no intentional oxidation is shown in Figure S2 in the Supporting Information, with much larger TMR of 135%. The XPS depth profile also confirmed the existence of richer oxygen content on the bottom electrode (Figure S3, Supporting Information). As the oxidation progresses, the added interfacial oxide produces more spin scattering and weakens the TMR. Interfacial oxidation is known to the magnetic tunnel junction industry and happens even under ultrahigh vacuum,[32] such as on the most widely used FeCo based alloys, and can reduce TMR due to increased spin scattering.[32–34] With even further oxidation, the TMR polarity eventually inverses. There are multiple ways that a negative spin polarization could happen, by competition between localized and delocalized electron states,[35,36] by resonant tunneling,[37,38] or by interfacial bonding changes.[38,39] Among these, the interfacial bonding mechanism is most relevant to our metal oxide interfaces, as the former are not interfacial and depend strongly on thicknesses or voltages.

The current-voltage ($I-V$) characteristics of junctions are illustrated in Figure 3d–f. Under applied electric fields, the devices show bi-stable resistance states, with the positive bias voltage switching the junction into a low resistance state (LRS) and the negative bias voltage returning the junction to a high resistance state (HRS). The abrupt jump in resistance is mainly governed by the energy barrier for Li ions migrating inside the LiF matrix, to be addressed at the end of this manuscript. Here the positive bias is defined as current flowing from the top electrode to the bottom electrode, and vice versa. The "set" and "reset" voltages are around 1.0 and −0.75 V, respectively, and the resistance ratio of the HRS versus LRS reaches more than 1000%. The $I-V$ curve is clearly nonlinear in the HRS, which suggests tunneling dominated transport. The fitted tunnel barrier heights are relatively low ($\approx$0.2 eV) because of the presence of defects necessary for ion migration. As a comparison, the

**ADVANCED
SCIENCE NEWS**
www.advancedsciencenews.com

**ADVANCED
ELECTRONIC
MATERIALS**
www.advelectronicmat.de

Figure 2. a) Schematic layout of an MTJ with (in nm): (100)-Si / MgO (10) / FeCo (8) / LiF (2.8) / FeCo (3) / Ti (50) / Pt (5), where the FeCo (8) and FeCo (3) / Ti (50) / Pt (5) are the bottom and top electrodes, respectively. We in situ pattern a $30 \times 30\ \mu m^2$ opening in an insulating MgO (red pad with a hole in the middle) to define the active junction area. b) Cross-sectional overview of the device. c) A high-resolution cross-sectional STEM image of the main section of the device. The red dashed lines are guide to the eyes to show the chemical boundaries. d) EELS mapping of individual elements across the marked area in Figure 1b.

$I–V$ is nearly linear in the LRS, indicating the diffusive nature in the electron transport, and fitting tunneling models to such curves (erroneously) produces much enlarged barrier heights.

We now look into the role of Li ion motion on the resistance switching. According to reported works on transition-metal oxide cathodes in lithium-ion batteries, the reactions of Li ions with Fe/Co occur at 1.5–2.5 V[40,41] and not accessible in our devices before permanent dielectric breakdown, while the reactions of Li ions with Fe/Co oxides occur in the range of 0.7–1.1 V[9,42–44] contributing to our observed results. Under a strong positive bias, the metal oxides tunnel barrier gives way to weaker Li_2O[45,46] by absorbing Li ions. More precisely, the interface loosely resembles (but not quite due to the low growth temperatures) the more complicated $Li_xM_yO_z$ compounds[47–49] (M is usually transition metal mixtures), and becomes more metal-oxide-like or more Li-oxide-like depending on the extent of Li ion insertion. There remains a possibility that the metal-oxide reduction happens on the metal-metal oxide interface rather than the metal oxide-LiF interface under the applied bias.[50] It is important to note that our oxide is on the ultrathin level, so the two interfaces are virtually the same interface as O can readily reach either side under almost any electromotive

force. Then the question becomes which side has better affinity with O electrochemically. The standard potentials (vs SHE) for $Fe^{2+} \rightarrow Fe$ and $Li^+ \rightarrow Li$ are −0.44 and −3.04 V, respectively, therefore it is more likely Li captures O and frees up Fe in the mean process, as we assumed in our model device.

As Li moves towards the interface, defects are also left behind inside LiF which significantly reduces the effective tunnel barrier heights. This can already induce considerable device resistance changes because quantum tunneling is exponentially sensitive to the tunnel barrier heights.[20,23,38,51–54] Furthermore, the defects left behind inside the barrier can mediate diffusive charge transport (resistor-like, linear $I–V$) without needing to tunnel across the energy barrier. Adding together, when the native oxides are reduced by the infusion of Li ions and the LiF matrix becomes defected with the outflow of Li ions, the device goes from the HRS into the LRS. This process is fully reversible under the application of opposite bias. As a comparison, in a near-pristine device with clean interfaces, no resistive switching is present up to the dielectric breakdown (Figure S2, Supporting Information).[55] This is because, even though the electric fields could be strong enough to trigger ionic motion, the ions still need a reservoir to occupy (cathode like places)
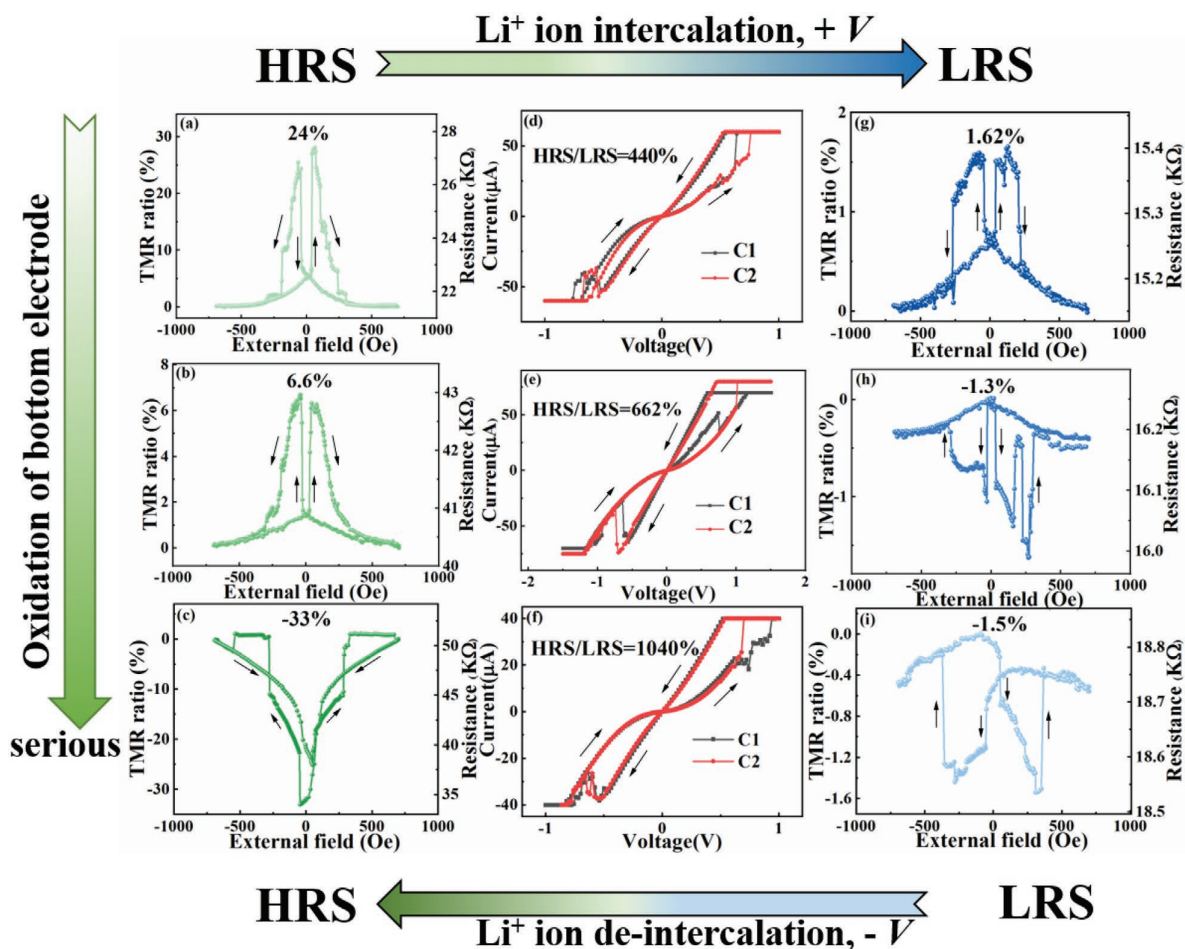
Figure 3. Magneto transport in FeCo/native oxide/LiF/FeCo tunnel junctions with progressive interface oxidation control. Measurements temperature was 77 K. The natural oxidation was achieved by exposing the bottom electrode to the base vacuum for 3, 6, and 12 h (from top to bottom panels, respectively). a–c) Typical TMR loops in HRS of the devices with different oxidation time. d–f) Typical I–V characteristics of the corresponding devices. To avoid permanent dielectric breakdown, a current limit was enforced on each measurement (thus the flat region) and increased gradually until the resistive switching occurred. g–i) Typical TMR loops in LRS of the corresponding devices.

in order to produce any stable and nonvolatile configurations. On the other end of the spectrum, when there is a thin layer of oxide but too thick LiF, resistive switching is present but no noticeable TMR is visible (Figure S4, Supporting Information), attributable to fully suppressed direct tunneling while only defect mediated hopping remains.

The modified tunnel barrier properties show up not only in junction resistances and resistive switching, but also in the resistance-temperature dependences. The resistance values in HRS and LRS both decrease with increasing temperatures (Figure S5, Supporting Information). It is worth noting that, the LRS resistance decreases by a factor of 5–10 as the temperature increases from 77 K to room temperature, much faster than the corresponding HRS resistance change (a factor of 1.2–1.9). Weaker temperature variation in the HRS indicates a robust, tunneling dominated behavior, whereas the stronger temperature dependence in the LRS is resultant of the defect-mediated transport (with low energy barriers) through the defective LiF and Li_2O barriers.

Figure 3g–i shows the TMR curves of the junctions at the LRS, displaying another two stable resistance states. Clearly, Li ion migration, evidenced from the resistive switching effect, and interfacial oxidation, seen from the weakening and reversal of TMR effect, coexist in our system. After applying a suitable positive bias voltage, Li ions are driven towards the interfacial oxides where surface redox happens, and in this process more defects are generated in the tunnel barrier because of the migration of Li ions. These not only lead to the observed LRS switching but also the significantly reduced TMR. This switching process is fully reversible at particular negative bias voltages, returning the device to the HRS. The most interesting scenario happens in the intermediate oxidation stage (Figure 3b,e,h), where interplay of these mechanisms are most pronounced. The sign of TMR can be tuned from positive to negative, and vice versa, with controllable ion motion. At HRS, direct tunneling between the two electrodes still dominates and is responsible for the overall

ADVANCED
SCIENCE NEWS
www.advancedsciencenews.com

ADVANCED
ELECTRONIC
MATERIALS
www.advelectronicmat.de

positive TMR. At LRS however, we need to note that there are only limited Li ions available for migration from the thin LiF, therefore not capable of fully reducing the oxide layer. As a result, the LRS not only has a highly defected barrier but also a partially-reduced metal oxide interface. Direct tunneling is mostly suppressed, and transport through the residual metal oxides (responsible for negative TMR) becomes dominant leading to a small (due to spin scattering) and negative TMR.

Next, we would like to address the possible complications of other elements, rather than Li, participating in the ion diffusion. According to our EELS mapping, F diffusion into the bottom electrode is clearly visible, likely during the process of growing LiF, some of the F atoms penetrate downward. Though Li is not visible under EELS, we can assume that some of Li may also migrate downward. However, we note, those elements embedded inside the metal matrix cannot feel the applied electric fields and therefore do not participate in our described ion-driven interfacial reactions. On the other hand, elements such as Li, F, and possibly O inside the composite tunnel barrier could potentially be driven out of place under applied electric fields. We performed first-principle calculations on the diffusion barriers for Li, F, and O inside the LiF matrix, and they turn out to be 0.78, 2.18, and 1.21 eV, respectively (Figure S7, Supporting Information). We can be assured that under mild electric fields, the dominant element mobile enough to move across the barrier is Li, as described in our prior discussions. We also note that these energy barriers are significantly higher than those in typical solid-state electrolytes, therefore ions are mostly frozen until strong enough driving electric fields are applied. Furthermore, under the proposed working principle, even if some other ions would migrate and trigger redox reactions at the interfaces, clear resistance and TMR changes are still expected in this device structure. In this system however, the likelihood of counter electrode reactions such as fluoride formation is hindered by the weak anion migration in the LiF matrix. As a control experiment, we fabricated devices under the same conditions with nearly identical stacking, except LiF being replaced by CaF_2, i.e., FeCo/native oxide/CaF_2/FeCo/Ti, For a nominal 2.8 nm CaF_2 barrier (Figure S8, Supporting Information). No resistive switching was observed in these junctions before dielectric breakdown kicking in ($\approx$2 V). Clearly, driving F ions requires significantly more efforts as they are indeed only partially mobilized.[56] This observation further highlights the important role of the Li ions, rather than the anions, as inferred in our system.

In the end, we summarize our tunnel junction's structural and behavioral similarity/distinction to an actual solid-state battery. LiF is analogous to a solid-state electrolyte, and the metal-oxide interface serves as the cathode. Electrochemistry between Li ions and cathode materials in response to strong enough electric field leads to the observed nonvolatile resistance changes. With our efforts keeping the electrolyte material thin, direct quantum tunneling still persists in the devices, leading to additional set of stable resistance states. Now it is time to point out our device' difference from an actual battery. Firstly, the lithium source for ions that can take part in the ion transport is very limited, and thus the actual charge storage is negligible. Secondly, large activation

barriers for ion migration exist for the chosen solid-state system, thus the created resistance states remain nonvolatile in the absence of applied fields and hence influencing the spin transports. Thirdly, when the electrolytes can accommodate the (small) ion number change and the resultant chemical valance change, they themselves can take care of the anode reactions and a true anode is no longer necessary.[57–59] In other words, LiF functions as the anode providing the ions needed in our system, ie, the corresponding anode reaction is $LiF - xe^- \rightarrow Li_{1-x}F + xLi^+$, and the resultant dielectric matrix also becomes more conducting leading to even lower resistance in the LRS. As a result, the field-driven ionic motion gives us additional control on the effective spin transport across these devices.

3. Conclusions

We demonstrate a battery-like magnetic tunnel junction with added ionic control and functionalities. In the LiF based tunnel devices, we show the coexistence of reversible, nonvolatile resistive switching and tunnel magnetoresistance effects, producing four well-defined resistance states on each device. Controlled oxidation is key to enabling interfacial redox reactions thus the ion-motion induced resistance changes. At the same time, the interfacial control allows one to actively tune the spin transport across the devices, making them much more versatile for applications.

4. Experimental Section

In this work, the battery-like magnetic tunnel junctions (MTJs) were in situ fabricated into micrometer dimensions on (100)-Si wafers, where the cross-bar geometry was obtained through shadow-masked electron-beam evaporation in a high vacuum system.[60,61] The system base pressure was 4×10^{-8} torr. In order to remove the native Si oxides and establish a hydrogen-terminated protective surface, the Si wafers were first ultrasonic cleaned in isopropyl alcohol, next dipped into 1% hydrofluoric acid for 90 s, and then immediately inserted into the loadlock chamber in less than a minute. The basic layout of the MTJs was (in nm): Si wafer / epi-MgO buffer (10) / $Fe_{50}Co_{50}$ (8) / LiF (2.8) / $Fe_{50}Co_{50}$ (3) / Ti (50) / Pt (5). The MgO (100) buffer layer was grown on the Si wafer at 300 °C to seed the subsequent growths. The elevated temperature was necessary to promote epitaxial correlation of MgO with the Si substrate,[61] while rest of the layers were all deposited at room temperature. Growth rates of all layers were in the range of 0.08–0.12 Å s^{-1} for better control and smoothness. The active junction area was 30×30 μm^2, defined by 10 nm MgO isolating everywhere else except the junction areas. For the hybrid samples, the MgO isolation was deposited after the bottom FeCo electrode deposition, then the bottom $Fe_{50}Co_{50}$ (8) layer was left exposed under the weak natural oxygen environment for various preset times before depositing the LiF layers. The MgO isolation layer deposition creates some interfacial oxidation, with notable pressure increase to the high 10^{-8} torr range. Then sitting in the stray oxygen partial pressure of 10^{-8} torr, the molecular impingement rate was equivalent to 10^{-3} monolayers/sec with a small fraction actually reacting, thus hours of exposure was needed to induce further controllable oxidation. This way the active junction area was exposed to oxidation whereby systematic modification was introduced to the first FeCo/LiF interface, forming the desired FeCoO$_x$-LiF composite barriers. For the pristine junctions, LiF was deposited before putting down the MgO isolation in order to

**ADVANCED
SCIENCE NEWS**
www.advancedsciencenews.com

**ADVANCED
ELECTRONIC
MATERIALS**
www.advelectronicmat.de

prevent accidental oxidation to the bottom electrodes. In the last step, 50 nm Ti and 5 nm Pt were deposited as the top electrode as well as a protection for the active junction regions. All transport properties were carried out with a two-terminal method at 77 K with devices fully submerged in liquid nitrogen. Serial resistances from the electrodes were only a few tens Ω and therefore neglected. The cross-sectional high-resolution scanning transmission electron microscopy (STEM) of the samples was performed with a JEOL 2200FS microscope at an accelerating voltage of 200 kV. The X-ray photoemission spectroscopy (XPS) depth profiling was performed with Omicron SPHERA II analyzer and Ar raster sputtering.

Supporting Information

Supporting Information is available from the Wiley Online Library or from the author.

Conflict of Interest

The authors declare no conflict of interest.

Data Availability Statement

The data that support the findings of this study are available from the corresponding author upon reasonable request.

[1] H. Kroemer, Nobel Lecture December 8, **2000**.

[2] F. Hellman, A. Hoffmann, Y. Tserkovnyak, G. S. D. Beach, E. E. Fullerton, C. Leighton, A. H. MacDonald, D. C. Ralph, D. A. Arena, H. A. Durr, P. Fischer, J. Grollier, J. P. Heremans, T. Jungwirth, A. V. Kimel, B. Koopmans, I. N. Krivorotov, S. J. May, A. K. Petford-Long, J. M. Rondinelli, N. Samarth, I. K. Schuller, A. N. Slavin, M. D. Stiles, O. Tchernyshyov, A. Thiaville, B. L. Zink, *Rev. Mod. Phys.* **2017**, *89*, 025006.

[3] S. Goswami, S. P. Rath, D. Thompson, S. Hedstrom, M. Annamalai, R. Pramanick, B. R. Ilic, S. Sarkar, S. Hooda, C. A. Nijhuis, J. Martin, R. S. Williams, S. Goswami, T. Venkatesan, *Nat. Nanotechnol.* **2020**, *15*, 380.

[4] S. Ikeda, K. Miura, H. Yamamoto, K. Mizunuma, H. D. Gan, M. Endo, S. Kanai, J. Hayakawa, F. Matsukura, H. Ohno, *Nat. Mater.* **2010**, *9*, 721.

[5] A. J. Tan, M. T. Huang, C. O. Avci, F. Buttner, M. Mann, W. Hu, C. Mazzoli, S. Wilkins, H. L. Tuller, G. S. D. Beach, *Nat. Mater.* **2019**, *18*, 35.

[6] J. M. Tarascon, M. Armand, *Nature* **2001**, *414*, 359.

[7] Y. Zhu, J. C. Gonzalez-Rosillo, M. Balaish, Z. D. Hood, K. J. Kim, J. L. M. Rupp, *Nat. Rev. Mater.* **2021**, *6*, 313.

[8] Z. Mustafa, D. Pravarthana, B. M. Wang, H. L. Yang, R. W. Li, *Phys. Rev. Appl.* **2020**, *14*, 014062.

[9] Q. Li, H. Li, Q. Xia, Z. Hu, Y. Zhu, S. Yan, C. Ge, Q. Zhang, X. Wang, X. Shang, S. Fan, Y. Long, L. Gu, G.- X. Miao, G. Yu, J. S. Moodera, *Nat. Mater.* **2021**, *20*, 76.

[10] J. C. Gonzalez-Rosillo, M. Balaish, Z. D. Hood, N. Nadkarni, D. Fraggedakis, K. J. Kim, K. M. Mullin, R. Pfenninger, M. Z. Bazant, J. L. M. Rupp, *Adv. Mater.* **2020**, *32*, 1907465.

[11] S. Z. Bisri, S. Shimizu, M. Nakano, Y. Iwasa, *Adv. Mater.* **2017**, *29*, 1607054.

[12] T. Tsuchiya, K. Terabe, M. Ochi, T. Higuchi, M. Osada, Y. Yamashita, S. Ueda, M. Aono, *ACS Nano* **2016**, *10*, 1655.

[13] X. J. Zhu, J. T. Zhou, L. Chen, S. S. Guo, G. Liu, R. W. Li, W. D. Lu, *Adv. Mater.* **2016**, *28*, 7658.

[14] C. Leighton, *Nat. Mater.* **2019**, *18*, 13.

[15] L. J. Wei, Z. Z. Hu, G. X. Du, Y. Yuan, J. Wang, H. Q. Tu, B. You, S. M. Zhou, J. T. Qu, H. W. Liu, R. K. Zheng, Y. Hu, J. Du, *Adv. Mater.* **2018**, *30*, 1801885.

[16] B. Cui, C. Song, F. Li, X. Y. Zhong, Z. C. Wang, P. Werner, Y. D. Gu, H. Q. Wu, M. S. Saleem, S. S. P. Parkin, F. Pan, *Phys. Rev. Appl.* **2017**, *8*, 044007.

[17] D. Yi, Y. Wang, O. M. J. van 't Erve, L. Xu, H. Yuan, M. J. Veit, P. P. Balakrishnan, Y. Choi, A. T. N'Diaye, P. Shafer, E. Arenholz, A. Grutter, H. Xu, P. Yu, B. T. Jonker, Y. Suzuki, *Nat. Commun.* **2020**, *11*, 902.

[18] N. Lu, P. Zhang, Q. Zhang, R. Qiao, Q. He, H. - B. Li, Y. Wang, J. Guo, D. Zhang, Z. Duan, Z. Li, M. Wang, S. Yang, M. Yan, E. Arenholz, S. Zhou, W. Yang, L. Gu, C. - W. Nan, J. Wu, Y. Tokura, P. Yu, *Nature* **2017**, *546*, 124.

[19] D. S. Kim, Y. D. Yun, J. S. Kim, Y. B. Kim, S. H. Jung, N. G. Deshpande, H. S. Lee, H. K. Cho, *ACS Nano* **2019**, *13*, 5987.

[20] M. Julliere, *Phys. Lett. A* **1975**, *54*, 225.

[21] J. S. Moodera, L. R. Kinder, T. M. Wong, R. Meservey, *Phys. Rev. Lett.* **1995**, *74*, 3273.

[22] T. Miyazaki, N. Tezuka, *J. Magn. Magn. Mater.* **1995**, *139*, L231.

[23] S. Yuasa, T. Nagahama, A. Fukushima, Y. Suzuki, K. Ando, *Nat. Mater.* **2004**, *3*, 868.

[24] S. S. P. Parkin, C. Kaiser, A. Panchula, P. M. Rice, B. Hughes, M. Samant, S.-H. Yang, *Nat. Mater.* **2004**, *3*, 862.

[25] S. Ikeda, K. Miura, H. Yamamoto, K. Mizunuma, H. D. Gan, M. Endo, S. Kanai, J. Hayakawa, F. Matsukura, H. Ohno, *Nat. Mater.* **2010**, *9*, 721.

[26] W.-G. Wang, M. Li, S. Hageman, C. L. Chien, *Nat. Mater.* **2012**, *11*, 64.

[27] A. Molinari, H. Hahn, R. Kruk, *Adv. Mater.* **2019**, *31*, 1806662.

[28] M. Nichterwitz, S. Honnali, J. Zehner, S. Schneider, D. Pohl, S. Schiemenz, S. T. B. Goennenwein, K. Nielsch, K. Leistner, *ACS Appl. Electron. Mater.* **2020**, *2*, 2543.

[29] V. Garcia, S. Fusil, K. Bouzehouane, S. Enouz-Vedrenne, N. D. Mathur, A. Barthélémy, M. Bibes, *Nature* **2009**, *460*, 81.

[30] E. Y. Tsymbal, A. Gruverman, V. Garcia, M. Bibes, A. Barthélémy, *MRS Bull.* **2012**, *37*, 138.

[31] Y. Wei, S. Matzen, C. P. Quinteros, T. Maroutian, G. Agnus, P. Lecoeur, B. Noheda, *npj Quantum Mater.* **2019**, *4*, 62.

[32] K. Tsunekawa, D. D. Djayaprawira, M. Nagai, H. Maehara, S. Yamagata, N. Watanabe, S. Yuasa, Y. Suzuki, K. Ando, *Appl. Phys. Lett.* **2005**, *87*, 072503.

[33] T. Moriyama, C. Ni, W. G. Wang, X. Zhang, J. Q. Xiao, *Appl. Phys. Lett.* **2006**, *88*, 222503.

[34] J. S. Moodera, G. X. Miao, T. S. Santos, *Phys. Today* **2010**, *63*, 46.

[35] M. Munzenberg, J. S. Moodera, *Phys. Rev. B* **2004**, *70*, 060402.

[36] T. H. Kim, J. S. Moodera, *Phys. Rev. B* **2004**, *69*, 020403.

[37] E. Y. Tsymbal, A. Sokolov, I. F. Sabirianov, B. Doudin, *Phys. Rev. Lett.* **2003**, *90*, 186602.

[38] E. Y. Tsymbal, O. G. Mryasov, P. R. LeClair, *J. Phys.: Condens. Matter* **2003**,*15*, R109.

[39] K. D. Belashchenko, E. Y. Tsymbal, M. van Schilfgaarde, D. A. Stewart, I. I. Oleynik, S. S. Jaswal, *Phys. Rev. B* **2004**, *69*, 174408.

[40] T. L. Zhao, L. Li, R. J. Chen, H. M. Wu, X. X. Zhang, S. Chen, M. Xie, F. Wu, J. Lu, K. Amine, *Nano Energy* **2015**, *15*, 164.

[41] F. Wang, H. C. Yu, M. H. Chen, L. J. Wu, N. Pereira, K. Thornton, A. Van der Ven, Y. M. Zhu, G. G. Amatucci, J. Graetz, *Nat. Commun.* **2012**, *3*, 1201.

[42] P. Poizot, S. Laruelle, S. Grugeon, L. Dupont, J. M. Tarascon, *Nature* **2000**, *407*, 496.

[43] H. S. Li, Z. Q. Hu, Q. T. Xia, H. Zhang, Z. H. Li, H. Z. Wang, X. K. Li, F. K. Zuo, F. L. Zhang, X. X. Wang, W. N. Ye, Q. H. Li, Y. Z. Long, Q. Li, S. S. Yan, X. S. Liu, X. G. Zhang, G. H. Yu, G. X. Miao, *Adv. Mater.* **2021**, *33*, 2006629.

[44] R. Dedryvere, S. Laruelle, S. Grugeon, P. Poizot, D. Gonbeau, J. M. Tarascon, *Chem. Mater.* **2004**, *16*, 1056.

[45] H. Kitaura, K. Takahashi, F. Mizuno, A. Hayashi, K. Tadanaga, M. Tatsumisago, *J. Electrochem. Soc.* **2007**, *154*, A725.

[46] H. Li, G. Richter, J. Maier, *Adv. Mater.* **2003**, *15*, 736.

[47] A. Moradpour, O. Schneegans, S. Franger, A. Revcolevschi, R. Salot, P. Auban-Senzier, C. Pasquier, E. Svoukis, J. Giapintzakis, O. Dragos, V. C. Ciomaga, P. Chretien, *Adv. Mater.* **2011**, *23*, 4141.

[48] Q. Hu, R. M. Li, X. J. Zhang, Q. Gao, M. Wang, H. L. Shi, Z. S. Xiao, P. K. Chu, A. P. Huang, *Sci. Rep.* **2019**, *9*, 5081.

[49] H. T. Li, Y. D. Xia, B. Xu, H. X. Guo, J. A. Yin, Z. G. Liu, *Appl. Phys. Lett.* **2010**, *97*, 012902.

[50] Z. He, R. V. Gudavarthy, J. A. Koza, J. A. Switzer, *J. Am. Chem. Soc.* **2011**, *133*, 12358.

[51] J. S. Moodera, T. S. Santos, T. Nagahama, *J. Phys.: Condens. Matter* **2007**, *19*, 165202.

[52] G.-X. Miao, J. Chang, B. A. Assaf, D. Heiman, J. S. Moodera, *Nat. Commun.* **2014**, 3682.

[53] G. X. Miao, M. Muller, J. S. Moodera, *Phys. Rev. Lett.* **2009**, *102*, 076601.

[54] C. Hellenthal, R. Heimbuch, K. Sotthewes, E. S. Kooij, H. J. W. Zandvliet, *Phys. Rev. B* **2013**, *88*, 035425.

[55] Q. Xue, Y. H. Yang, Z. W. Gao, F. Liu, Q. Li, S. D. Li, G. X. Miao, *Appl. Phys. Lett.* **2016**, *109*, 192407.

[56] J. Senegas, S. H. Pulcinelli, *J. Fluorine Chem.* **1988**, *38*, 375.

[57] B. Lei, N. Z. Wang, C. Shang, F. B. Meng, L. K. Ma, X. G. Luo, T. Wu, Z. Sun, Y. Wang, Z. Jiang, B. H. Mao, Z. Liu, Y. J. Yu, Y. B. Zhang, X. H. Chen, *Phys. Rev. B* **2017**, *95*, 020503.

[58] U. Bauer, L. Yao, A. J. Tan, P. Agrawal, S. Emori, H. L. Tuller, S. van Dijken, G. S. D. Beach, *Nat. Mater.* **2015**, *14*, 174.

[59] C. Bi, Y. Liu, T. Newhouse-Illige, M. Xu, M. Rosales, J. W. Freeland, O. Mryasov, S. Zhang, S. G. E. Velthuis, W. G. Wang, *Phys. Rev. Lett.* **2014**, *113*, 267202.

[60] X. Y. Gao, Q. Li, S. D. Li, J. Xu, Y. Z. Qin, X. J. Shi, S. S. Yan, G. X. Miao, *J. Alloys Compd.* **2016**, *662*, 79.

[61] G. X. Miao, J. Y. Chang, M. J. van Veenhuizen, K. Thiel, M. Seibt, G. Eilers, M. Muenzenberg, J. S. Moodera, *Appl. Phys. Lett.* **2008**, *93*, 142511.